SCIENCE CHINA
Life Sciences

•RESEARCH PAPER•

October 2021 Vol.64 No.10: 1661–1676
https://doi.org/10.1007/s11427-020-1836-7

Longitudinal single-cell RNA-seq of hESCs-derived retinal organoids

Shaojun Wang[2,3], Sergio Poli[4#], Xiaoliang Liang[4] & Guang-Hua Peng[1,5*]

[1]*Laboratory of Visual Cell Differentiation and Regulation, Basic Medical College, Zhengzhou University, Zhengzhou 450001, China;*
[2]*Department of Ophthalmology, First medical center of Chinese PLA General Hospital, Beijing 100853, China;*
[3]*Department of Ophthalmology, Fifth medical center of Chinese PLA General Hospital, Beijing 100071, China;*
[4]*Division of Pulmonary and Critical Care Medicine, Brigham and Women's Hospital, Harvard Medical School, Boston 02115, USA;*
[5]*Department of Pathophysiology, Basic Medical College, Zhengzhou University, Zhengzhou 450001, China;*
[#]*Current address: Division of Internal Medicine, Mount Sinai Medical Center, Miami, Florida 33140, USA*

Received August 3, 2020; accepted October 13, 2020; published online January 27, 2021

Human retina development involves multiple well-studied signaling pathways that promote the genesis of a wide arrange of different cell types in a complex architectural structure. Human embryonic stem cells (hESCs)-derived retinal organoids could recapitulate the human retinal development. We performed single-cell RNA-seq of retinal organoids from 5 time points (D36, D66, D96, D126, D186) and identified 9 distinct populations of cells. In addition, we analyzed the molecular characteristics of each main population and followed them from genesis to maturity by pseudotime analysis and characterized the cell-cell interactions between different cell types. Interestingly, we identified insulin receptor (INSR) as a specifically expressed receptor involved in the genesis of photoreceptors, and pleiothropin (PTN)-protein tyrosine phosphatase receptor type Z1 (PTPRZ1) as a mediator of a previously unknown interaction between Müller and retinal progenitor cells. Taken together, these findings provide a rich transcriptome-based lineage map for studying human retinal development and modeling developmental disorders in retinal organoids.

human embryonic stem cell, photoreceptor cell, single cell RNA sequencing, retinal pigment epithelium, retinal organoid

Citation: Wang, S., Poli, S., Liang, X., and Peng, G.H. (2021). Longitudinal single-cell RNA-seq of hESCs-derived retinal organoids. Sci China Life Sci 64, 1661–1676. https://doi.org/10.1007/s11427-020-1836-7

INTRODUCTION

The human retina is a highly-evolved complex and unique structure. Stem cell-based models of human retina development have been designed to elucidate and treat retinal degenerated disease (da Cruz et al., 2018; Schwartz et al., 2015; Shen et al., 2020). In particular, great efforts have been made to generate transplantable photoreceptors and retinal pigment epithelial (RPE) cells from human embryonic stem cell (hESCs) line (Zhu et al., 2018). It is essential to fully illustrate the developmental character of these cells.

The molecular networks that drive fate decisions and the development of retinal cells, especially photoreceptor and RPE cells, are not fully understood. Single-cell transcriptomics could reveal these gene networks with high-dimensional molecular characterization at single-cell scale (Han et al., 2018; Klein et al., 2015; Liu et al., 2018; Macosko et al., 2015), as shown in hESCs-derived brain organoid (Yao et al., 2017; Zhong et al., 2018). Many studies have been performed describing the rodent organ development (Dulken et al., 2017; Farrell et al., 2018; La Manno et al., 2016; Tasic et al., 2016; Treutlein et al., 2014; Wagner et al., 2018; Wu et al., 2017; Zeisel et al., 2018; Zeisel et al., 2015) and organ cell component (Han et al., 2018; Paul et al.,

*Corresponding author (email: ghp@zzu.edu.cn)

2015; Zhou et al., 2016). Single-cell RNA sequencing (scRNA-seq) has major effect on the biological field (Camp et al., 2018), including the study of retina. Comprehensive classification of retinal bipolar cells has been performed at the single-cell scale (Shekhar et al., 2016). Recently, scRNA-seq was used to classify the components of the macular retina cell population of macaques (Peng et al., 2019). In parallel, recent progress in modeling human retinal development from pluripotent stem cells (Kuwahara et al., 2015; Nakano et al., 2012) has allowed the supply of human retinal tissue at developmental stages that are typically unavailable. These retinal organoids from hESCs efficiently recapitulate retinogenesis (Völkner et al., 2016), and have been applied to generate photoreceptor cells (Gonzalez-Cordero et al., 2017) and investigate the gene regulatory networks of human retinal development (Kaewkhaw et al., 2015). Recent efforts to characterize the retina at the single-cell level have been published (Collin et al., 2019; Mao et al., 2019; Phillips et al., 2018). However, the genesis of each cell type, the dynamic maturation process and cell interactions in the retinal organoid have not been fully determined.

Here, we present a study of the scRNA-seq characterization of the early human retina cell development of a retinal organoid model. We computationally identified cell types, predicted their lineage relationships, explored cellular interactions and experimentally confirmed predictions using multiplex immunofluorescence analysis.

RESULTS

In vitro model of human retina cell development

We employed an *in vitro* model of human retinal development based on the differentiation of hESCs, which was adapted from previous protocols (Kuwahara et al., 2015). hESCs could form colonies and were positive for OCT4, SOX2, SSEA-4 and TRA-1-60 (Figure 1A). hESCs could generate self-organized stratified neural retina (NR) and RPE cells using a three-dimensional culture technique. We successfully applied the self-organization culture approach of hESCs to recapitulate retinal development *in vitro*. Using induction-reversal culture combined with BMP4-triggered

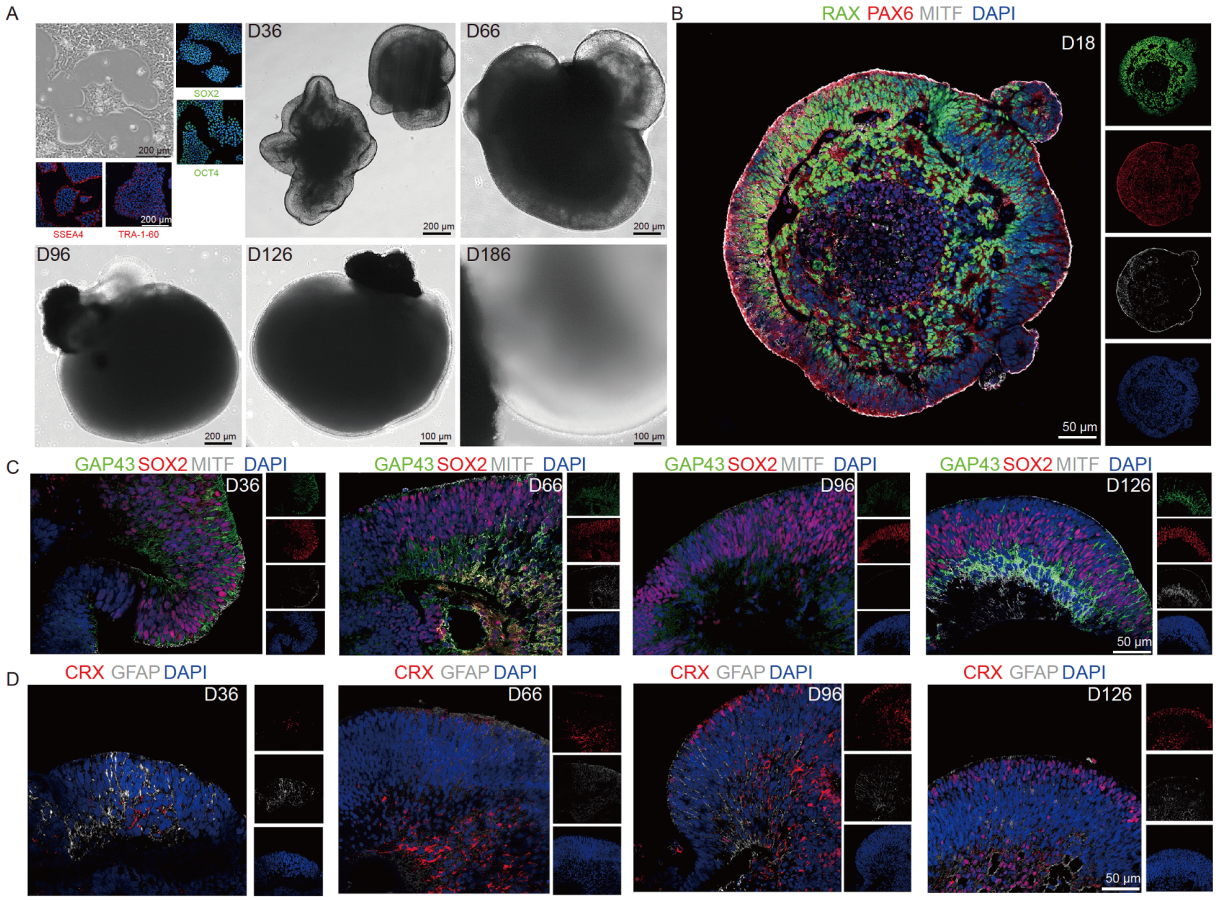

Figure 1 *In vitro* generation of retinal organoid from hESCs. A, Bright field view hESCs colony; Immunostaining of OCT4 (green), SOX2 (green), SSEA4 (red) and Tra-1-60 (red); DIC image of retinal organoid from D36, D66, D96, D126 and D186 after differentiation. B, Multiple immunostaining of RAX (green), PAX6 (red), MITF (gray) and DAPI (blue) in retinal organoids at D18. C, Multiple immunostaining of GAP43 (green), SOX2 (red), MITF (gray) and DAPI (blue) of retinal organoid at D36, D66, D96, and D126. D, Multiple immunostaining of CRX (red), GFAP (gray) and DAPI (blue) of retinal organoid at D36, D66, D96 and D126.

highly selective retinal differentiation, we observed retinal self-organization in 3D hESCs culture (Figure 1A). Most of the BMP4-induced epithelium was positive for RAX and PAX6, moreover, MITF could be detected in the margin at day 18 (Figure 1B). Next, we observed the expression of SOX2, GAP43, MITF, CRX and GFAP at D36, D66, D96, and D126 (Figure 1C and D). We found that the SOX2 positive cells gradually migrated in the inner layer of the retinal layer, especially at D126. CRX- or GFAP-positive cells appeared at D36 and gradually increased during the differentiation process. Furthermore, we profiled five different stages (D36, D66, D96, D126 and D186) of our *in vitro* differentiation protocol and established its reproducibility across replicate differentiations by analyzing populations of cells from each time point using scRNA-seq analysis.

Single-cell profiling and identification of cell types in the retinal organoid

ScRNA-seq data were harvested from 80,199 individual cells from 5 independent time points (D36, D66, D96, D126 and D186) of the differentiation process (Figure 2A). A total of 89% of the transcripts was mapped to a single locus and the median number of genes per cell was 4,378. To classify the major cell types in the retinal organoids, we analyzed cells through a standard pipeline using Seurat R package, version 2 (Butler et al., 2018). A total of 9 cell populations were identified: RPE cells, retinal progenitor cells (RPCs), retinal ganglion cells (RGCs), including a subset labeled mature RGCs, photoreceptor precursor cells (PCs), Müller cells (MCs), cone photoreceptor cells, rod photoreceptor cells, fibroblast cells, and blood vessel cells (Figure 2A). Canonical markers used to distinguish the cell clusters were *MITF* and *PMEL* as markers for RPE cells, *RCVRN*, *NRL*, *PDE6H* and *NR2E3* for photoreceptor cells, *SOX2*, *SFRBP2* for RPCs, *GFAP*, *S100B*, *APOE* for MCs, *GAP43*, *SNCG* for RGCs (Figure 2B). The proportion of progenitor cells dropped as cells differentiate, while the proportion of photoreceptor increased, and photoreceptor precursors emerged at day 36 and gradually increased. The ganglion cells appeared early at D36, and their abundance declined over time. Cone photoreceptor cells were predominantly derived from D186, and rod photoreceptor cells from both D126 and D186 (Figure S1 in Supporting Information). Different markers of each population are shown in the expression heatmap in Figure 2C. Combination analysis of the human fetal retina (Hu et al., 2019) and retinal organoid showed that the main neural retinal populations share similar cluster characteristics (Figure 2D).

Identification of lineage trajectories and cell interactions

To analyze the global connectivity and the trajectory topology of the dataset, we implemented partition-based graph abstraction (PAGA) and obtained the connectivity map of the clusters, enabling the identification of highly connected nodes that may represent differentiation status (Figure 3A). We identified four different groups of neighboring nodes through diffusion propagation network analyses that represent differentiation trajectories with specific lineage commitment (Figure 3B). To better identify the molecular changes that occur during the developmental transition and to establish a diffusion pseudotime (DPT), we applied diffusion mapping and reanalyzed uniform manifold approximation and projection (UMAP) coordinates with positions initialized from PAGA (Figure 3C and D). We identified different clusters with terminal phenotypes that corresponded to terminal nodes of the lineage trajectory subnetworks (Figure 3A) and assessed the expression as a function of pseudotime of canonical markers, confirming the molecular development of four different cell types (Figure 3E).

By using iTALK R package (Wang et al., 2019), we calculated the cell-cell ligand receptor interactions, which are shown in Figure 4A. We found robust cell interactions between RPE cells and PCs and identified pleiothropin (PTN)-protein tyrosine phosphatase receptor type Z1 (PTPRZ1) as a previously described interaction between MCs and RPCs (Hu et al., 2019) (Figure 4A). The top interactions by groups (cytokines, growth factors, checkpoints and others) were shown in Figure 4B. Insulin receptor (INSR) is a tyrosine kinase receptor predominantly expressed in cluster 30 (PC), and it establishes interactions with ligand calmodulin 2 (CALM2) in clusters 11 and 21 (PC), and 7 (RPC) and 3 (RGC) (Figure 4C).

Subclustering RPCs to identify retinal stem cells

We performed a subcluster analysis of RPCs (Figure 5A) and identified a cluster of RPCs (Figure 5B) with increased expression of SOX2, SRFBP2, RAX, PAX6 and NESTIN, which are markers previously shown to be associated with retinal stem cells. To characterize this population, we performed differential expression (DE) analysis against all other RPC clusters, which showed multiple genes related to stemness, such as the ones mentioned before and others like SIX6, FGF19, IGFBP2. Interestingly, multiple genes related to endocrine hormones, such as PTH2, CCK, MDK, ARGLU1, were upregulated in this population, suggesting a role of these hormones in the signaling involved in retinal differentiation. MTRN, previously shown to regulate glial cell differentiation, was also upregulated in this population. Furthermore, we identified multiple surface molecule-coding genes such as FLRT2, FLRT3, PCDH9, PCDH7 and DLK1 that have not been previously described. This may help to identify and isolate these retinal stem cells (Figure 5C). By using SCORPIUS, we identified gene expression changes as

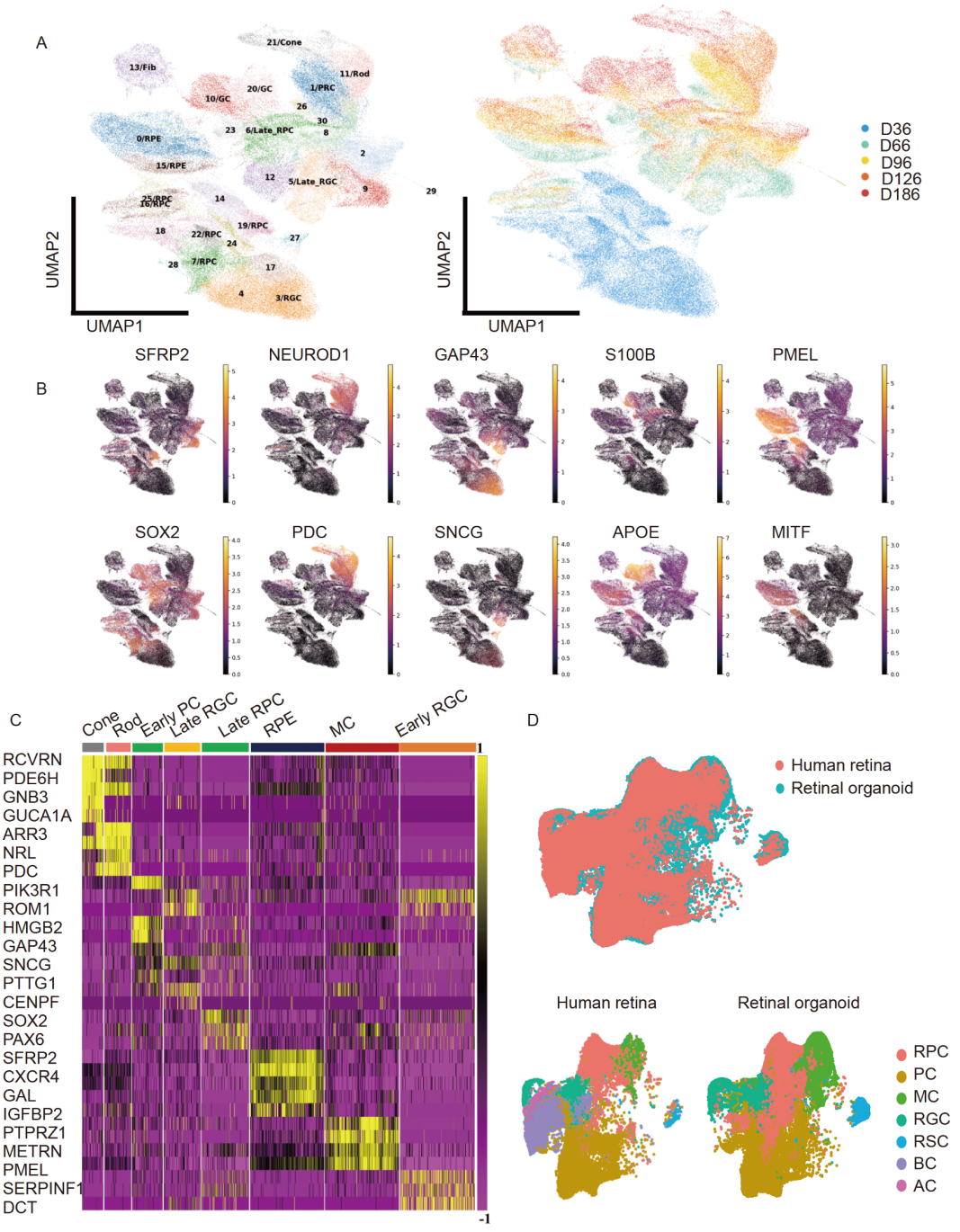

Figure 2 Single-cell RNA-seq analysis of human retinal organoid. A, UMAP plots of the single-cell retinal organoid dataset, labeled by clusters and sample timepoints. B, Multiple feature plots showing the expression of hallmark genes for each specific cell subpopulation. C, Heatmap of top genes for each of the mature cell populations. D, UMAP plots of the single cell organoid dataset compared with the human retinal dataset by Hu et al. (2019).

a function of the pseudotime trajectory and cluster them in modules based on their expression patterns across pseudotime. Two modules of genes were more highly expressed at pseudotime 0, the first module included genes mostly related to the cell cycle and genes in the second were associated with the Wnt signaling pathway (consistent with literatures describing the role of this pathway in retinogenesis) or the Apelin signaling pathway (previously described as a critical pathway for angiogenesis because knockout of apelin gene resulted in a delay in the development of retinal vasculature). Two more modules were associated with increased expression at pseudotime 1 and related to ferroptosis, Parkin-mediated proteasomal systems, lipid metabolism, PPAR alpha, statin, and prostaglandin synthesis pathways. These modules were also associated with ERK and spinal cord injury ontologies (Figure 5D).

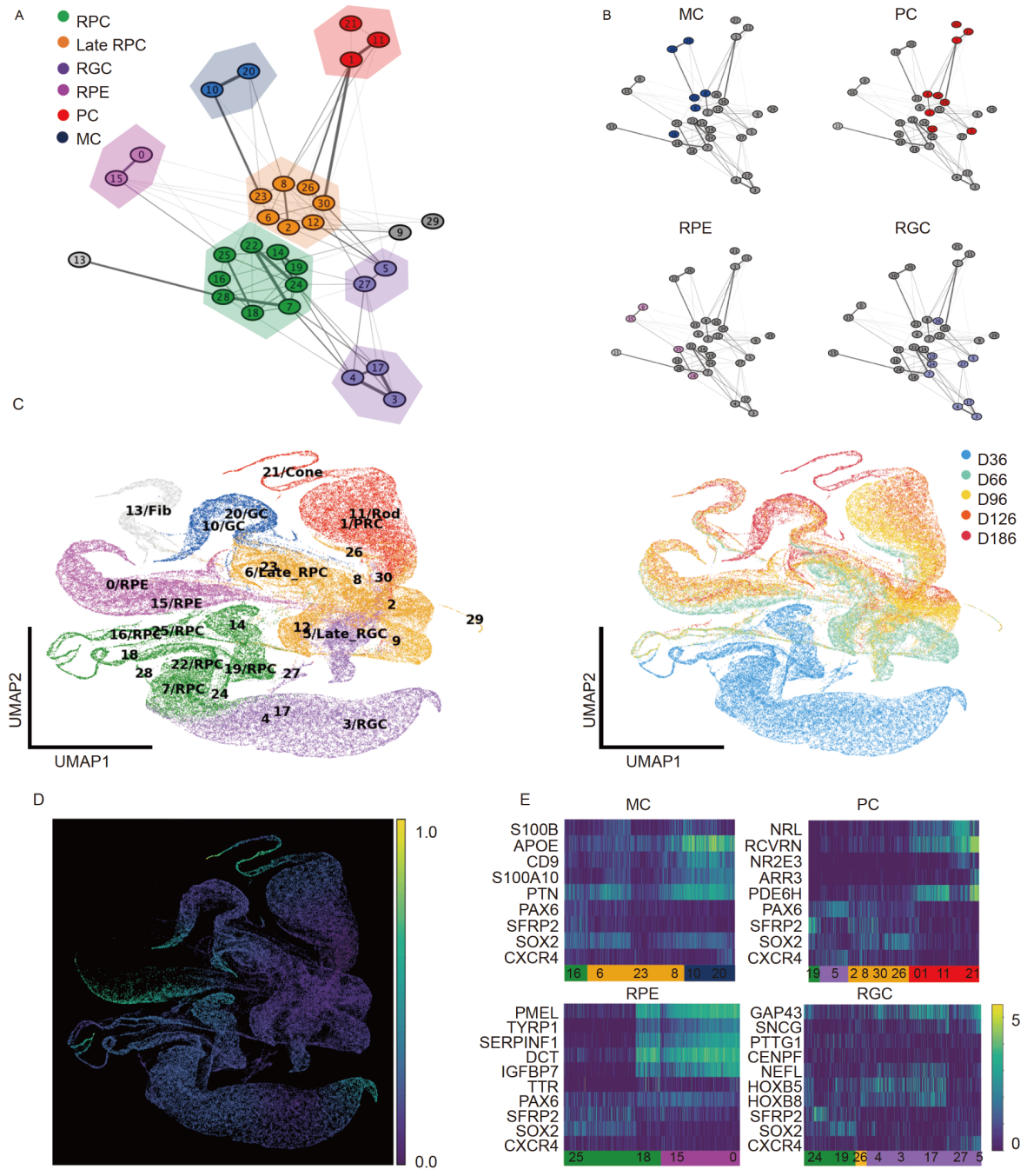

Figure 3 Pseudotime analysis of human retinal organoid cells. A, PAGA network plot of the retinal organoid dataset, labeled by cell subpopulations. Each node represents a cluster shown in Figure 2A. B, Trajectory path of specific cell types. Highlighted, the nodes (cell clusters) represented in each differentiation trajectory pathway. C, UMAP of retinal organoid dataset following diffusion map implementation, labeled by cell clusters and sample timepoints. D, Heatmap of the organoid dataset sorted by diffusion pseudotime distance across the UMAP representation. E, Heatmaps of genes subsetted by clusters in each trajectory pathway, which was sorted by pseudo time distance.

RPE cell genesis and maturation

After subclustering cells corresponding to the RPE linear trajectory were identified by the PAGA network analysis (Figure 6A), we performed DE analysis on the most immature cluster (cluster 18) that originated exclusively from D36, and the most mature cluster (cluster 0) that comprised samples from D96 and D126. Furthermore, the expression of canonical markers, such as MITF, PMEL, TYRP1, indicated a gradient of expression from D36 to D126, once again showing that these cells are part of the same lineage trajectory and that these canonical markers were upregulated across the maturation process (Figure 6A). For samples from cluster 18, DE analysis revealed genes related to cell cycle, such as CDK1, CCNB1, CCNB2, MKI67, UBE2S, TOP2A. When we filtered for surface molecules, GPC3 gene that

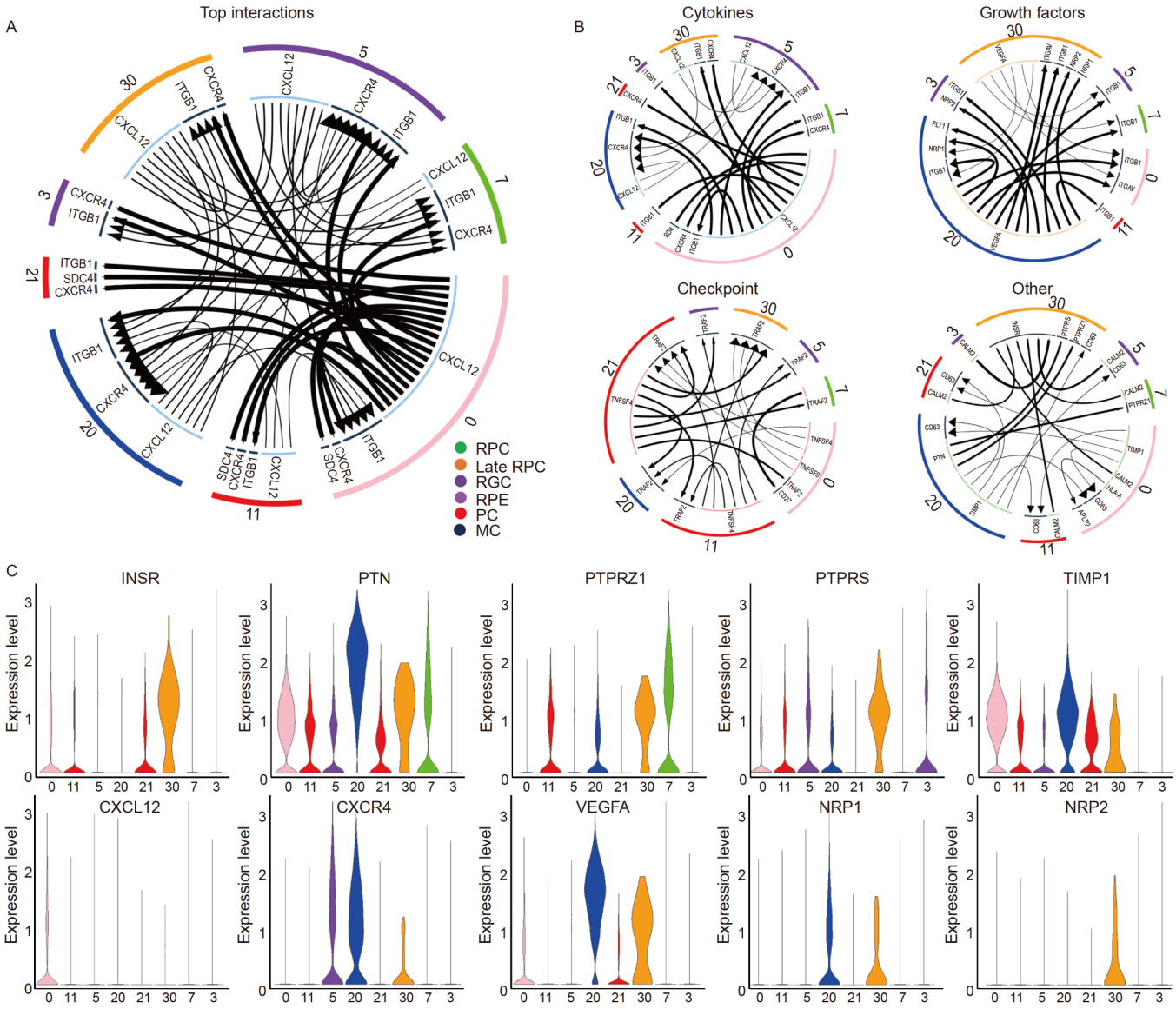

Figure 4 Ligand-receptor-mediated cell interaction in the retinal organoid. A, Top L-R interactions between all subgroups. B, L-R interactions between subgroups. C, Violin plots of the expression of the top differentially expressed L-R pairs by cell type.

encodes a small glycoprotein has been shown to have a role in the regulation of cell survival during embryo development through modulation of the Wnt pathway (De Cat et al., 2003). PTPRZ1, a receptor that was previously shown to be involved in the early stages of RPE development, interacts with retinal cells through PTN and MDK (Hu et al., 2019), CNTNAP2, TTYH1, THY1, NCAM1, and GPM6B, were the top molecules differentially expressed in these immature RPE, compared to more mature RPE cells. These genes are previously undescribed molecules of RPE cell progenitors (Figure 6B). The DE analysis of Cluster 0, or more mature cells, showed overexpression of CST3, TIMP3, PTGDS, COL8A1, TTR, and GPNMB (Figure 6B). The pseudotime analyses demonstrated an enrichment of expected processes in more mature cells, such as phototransduction, tyrosine metabolism, regulation of lipid metabolism, and unexpected processes such as necroptosis, nitrogen metabolism, arginine biosynthesis and Il-1 signaling pathway (Butler et al., 2015; Hu et al., 2019; Zurdel et al., 2002) (Figure 6C).

Molecular characterization of mature and immature PCs

To reveal the diversity of PCs in human retinal organoid, we performed subcluster analyses of cells that were part of the PC differentiation path and identified two different clusters of cells with gene expression suggestive of mature cones (21) and rods (11). We also identified a cluster of cells that form the most immature cluster, deriving exclusively from D66 (cluster 30) and having a unique set of overexpressed surface

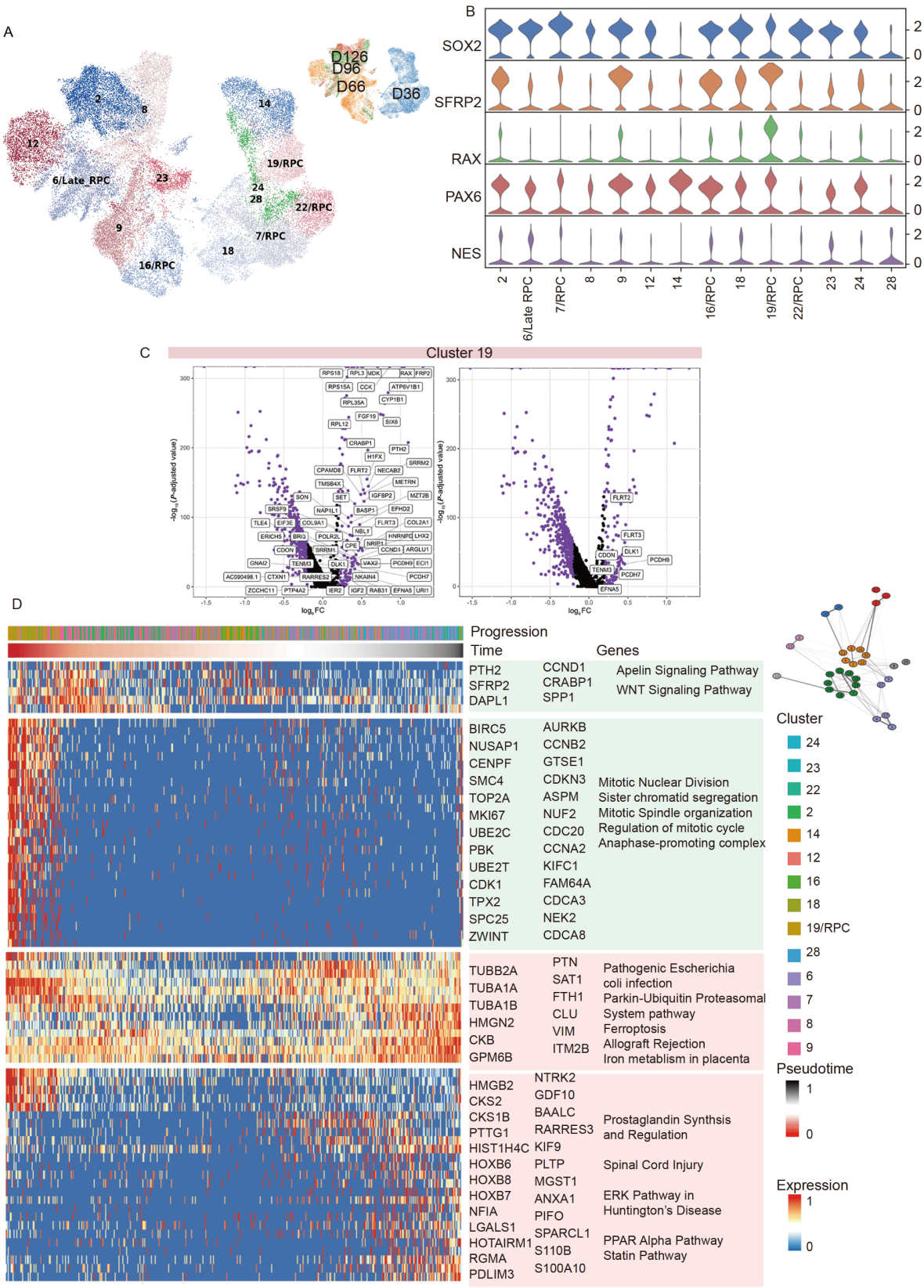

Figure 5 Subset analysis of RPCs from human retinal organoids. A, UMAP plot of the RPC cluster subset labeled by cluster. B, Violin plot of gene expression of the TF associated with RSCs: SOX2, SFRP2, RAX, PAX6 and NES. C, Volcano plot showing differentially expressed genes from cluster 19, the cluster with the highest expression of the previously mentioned TFs. D, Expression heatmap sorted by diffusion pseudotime distances calculated by SCORPIUS, showing that top genes (P value<0.05) grouped by modules were differentially expressed as a function of pseudotime. Gene ontologies were determined for each of the correlated-gene modules.

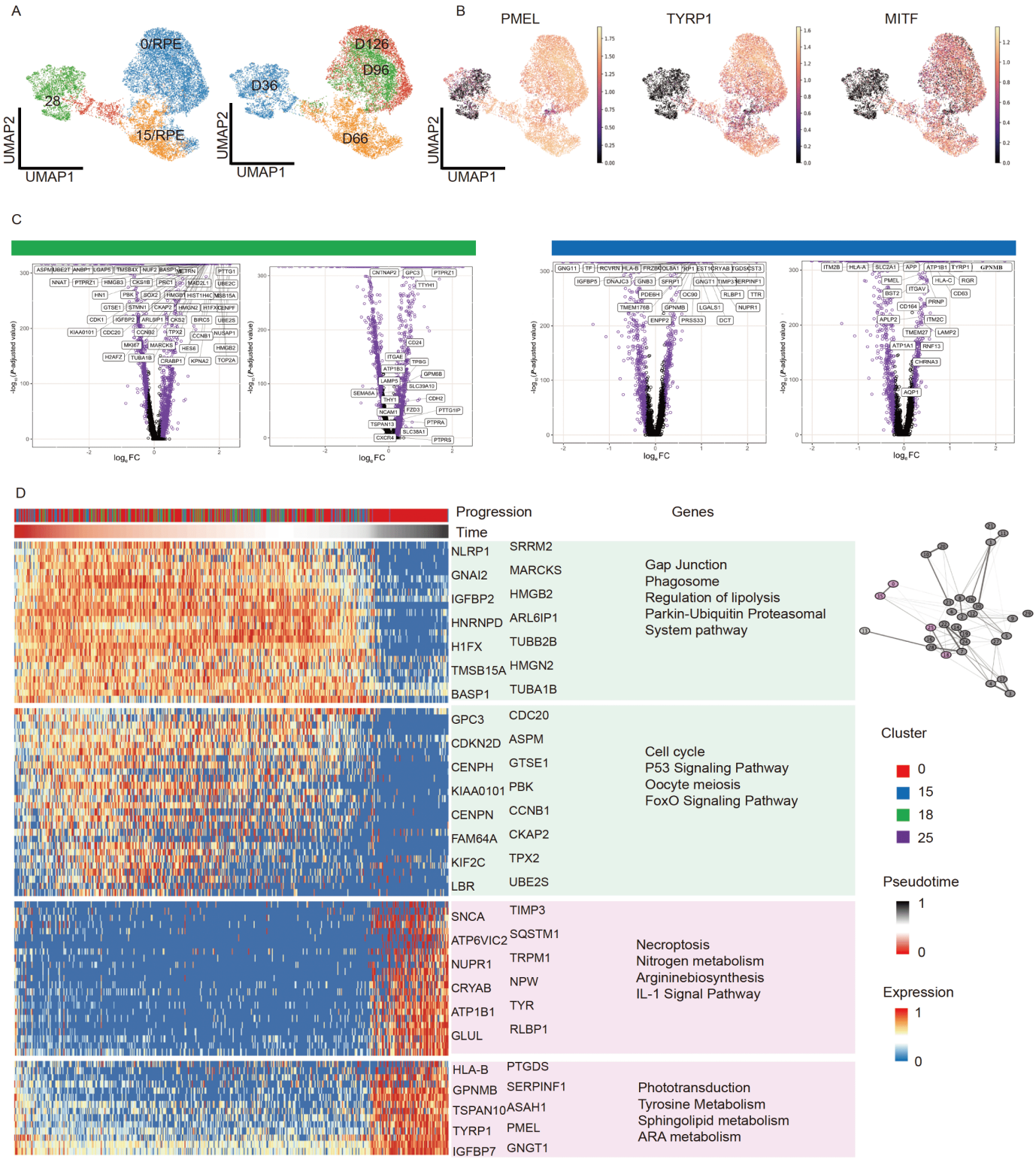

Figure 6 Subset analysis of RPE cells from human retinal organoids. A, UMAP plot of the RPE cluster subset labeled by clusters and time points. B, Feature plots showing the expression of hallmark genes of RPE cells: PMEL and TYRP1 and MITF. C, Volcano plot showing differentially expressed genes from cluster 18 and cluster 0, the most extreme clusters of differentiation process of RPE cells (representing most immature and mature cells, respectively). D, Expression heatmap sorted by diffusion pseudotime distances calculated by SCORPIUS, showing that top genes (P value<0.05) grouped by modules were differentially expressed as a function of pseudotime. Gene ontologies were determined for each of the correlated-gene modules.

markers, such as VEGFA, INSR, and NKTR (Figure 7B). INSR has been previously shown to be expressed in the retina (Hitchcock et al., 2001; Otteson et al., 2002). By pseudotime analysis, we identified processes associated with

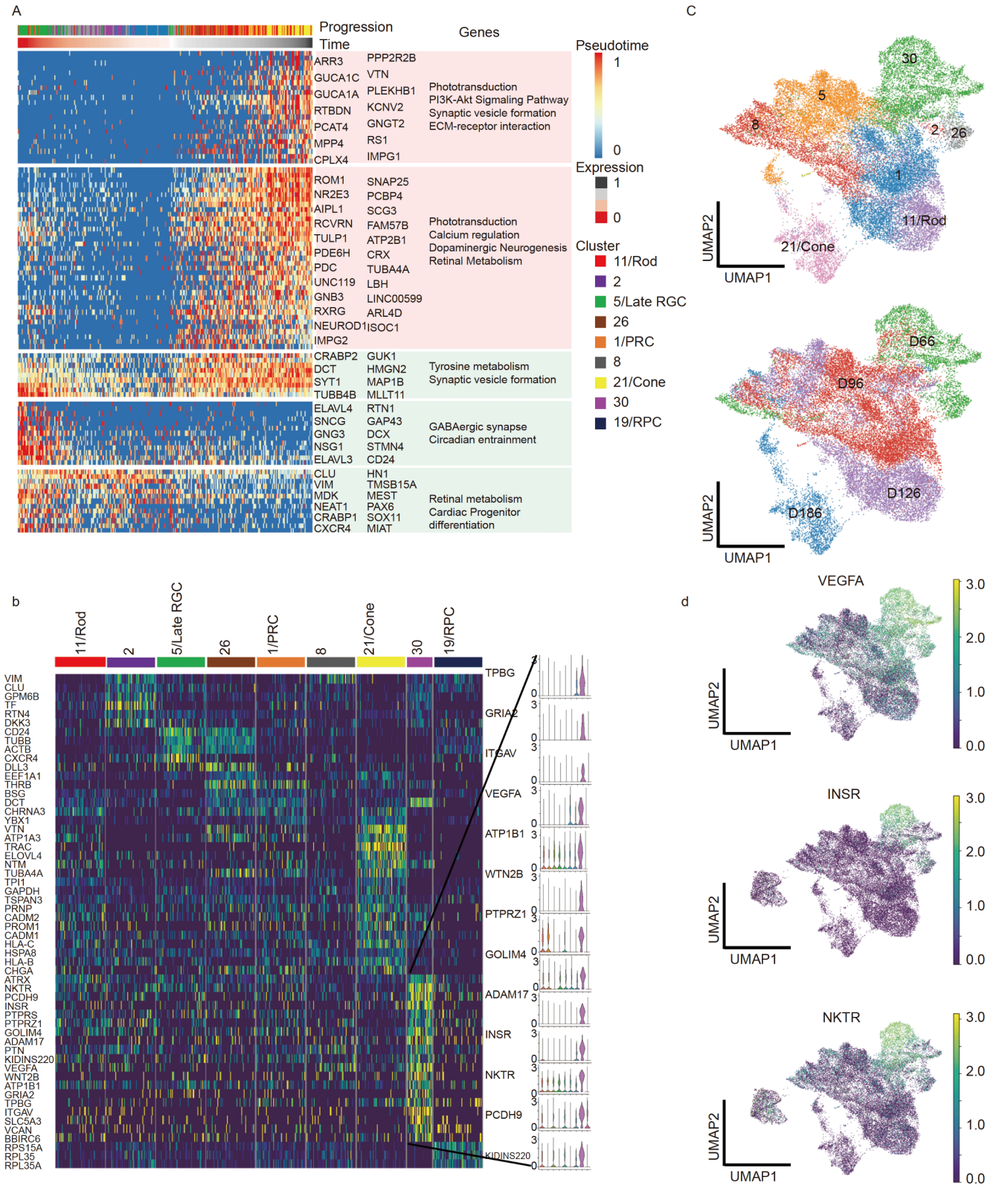

Figure 7 Subset analysis of PCs from human retinal organoids. A, Expression heatmap of PCs sorted by diffusion pseudotime distances calculated by SCORPIUS, showing that top genes (P value<0.05) grouped by modules were differentially expressed as a function of pseudotime. Gene ontologies were determined for each of the correlated-gene modules. B, Expression heatmap of surface molecule-coding genes, which are classified by cell cluster. C, UMAP plot of the PC cluster subset labeled by cluster and sample time point. D, Feature plot showing the gene expression of the top three surface-molecule coding genes, showing specificity to certain cell clusters and time point.

mature cell states, such as retinal metabolism, photo-transduction, dopaminergic neurogenesis and PI3k-Akt signaling pathway (Figure 7A). Furthermore, we explored the role of INSR during the PC mature process. We applied the INSR specific inhibitor BMS-754807 at 1 μmol L^{-1} from D66 to D96. The mRNA levels of genes (NRL, CRX, NR2E3, NEUROD1, BLIMP1, ARRESTIN3, AIPL1, RECOVERIN, RXRG, PDC and ROM1) involved in the development of retinal photoreceptor cells in the BMS-754807 group were higher (P value<0.01) than those in the control group at D96 (Figure 8A). To confirm these findings, we explored protein expression by immunofluorescence staining of CRX and found that these proteins were significantly overexpressed compared with those in the controls (Figure 8B). To further validate the findings, we assessed RHODOPSIN and OPNSW in the BMS-754807 group and found that they were also overexpressed compared to those in the controls, indicating that the development of both cones and rods is enhanced by the blocking of INSR (Figure 8C).

Retinal ganglion cells: the intrinsically photosentive RGCs

To study the heterogeneity of ganglion cells, we followed the same approach in the previously mentioned populations. We subclustered cells with gene expression signatures that were associated with known ganglion cell hallmark genes, such as GAP43 and SNCG (Figure 9A). We identified two different subsets of cells, the first arising predominantly from D36 or more immature cells and the second arising from D66 or more mature cells. Interestingly, SNCG is a marker of mature and more differentiated ganglion cells. We performed DE analysis on the two populations and found significant expression of an orphan RAR nuclear receptor (RORB), which is associated with retinoid metabolism and implicated in the maturation of neuron cells. Specifically, RORB is related to maturation of photoreceptor cells, with known downstream effects such as activation of the NRL transcription factor-mediated pathway. Furthermore, in the trajectory inference analysis, the mature RGC subpopulation was a part of the photoreceptor differentiation pathway, being an intermediate cell type in the emergence of cones and rods. These cell subsets may represent the ganglion circadian photosensitive cell, melanopsin producers, which share some photosensitivity functions with classic photoreceptor cell types (Berson, 2003). This result may be further supported by the expression of PRPH gene by these cells, an intermediate filament associated with long projections to distant structures, as ganglion cells axons are closely related to CNS deep structures and is a marker of intrinsically photosensitive RGCs, as described before in the mouse single cell RNA seq (Laboissonniere et al., 2019).

DISCUSSION

We demonstrated a comprehensive characterization of human retinal cell types generated from hESCs and defined multiple different cell types consisting of progenitors, neuronal and glial cell types. We determined the transcriptomic signature of RPCs, PCs and RPE cells from emergence to maturity. We also demonstrate that retinal organoid could be used to assess the key development process of the human retina at the single-cell scale. These findings will be beneficial for regenerative medicine.

The recently developed hESCs-derived retinal organoid enhanced the study of human retinal development (Gonzalez-Cordero et al., 2017; Kuwahara et al., 2015; Nakano et al., 2012). However, the similarity between the retinal organoid and the human fetal retina is not well explored. By combining our analysis with Tang's fetal retina dataset, we found a high correlation of the RPCs, RGCs, PCs, MCs between retinal organoid and human fetal retina (Hu et al., 2019). Moreover, in our study, we fully analyzed the differentiation process of retinal cells from hESCs at the single-cell scale. We found no unwanted hESCs residues by scRNA-seq and immunofluorescence; moreover, the 3D organoid cells from D36, D66, D96, D126 and D186 did not form tumors when injected subcutaneously into NOD SCID mice (Figure S2 in Supporting Informaion). The results demonstrate the complete differentiation of hESCs in the 3D organoid model.

Several pioneer studies have investigated the differentiation process of retinal cells from hESCs by using bulk RNA sequencing and provided important knowledge for the field (Kaewkhaw et al., 2015). By using scRNA-seq, we dissected the cell type constitution at different differentiation stage of retinal organoids, from D36 to D186. The cell types we identified conform with those identified by other groups (Collin et al., 2019; Kim et al., 2019; Mao et al., 2019; Phillips et al., 2018). In addition, we identified the transcriptional signature of RSCs, RPE cells, RPCs, RGCs, cone-photoreceptor cells, rod-photoreceptor cells and MCs. We also traced the RPE cells, RPCs and PCs from emergence to maturity and depicted the key regulation signal pathways. All this information will be beneficial for generating seed cells for transplant; for example, from this information, we could determine the time point to isolate RPE cells or PCs as seed cells.

We have classified the genesis process of photoreceptor cells and identified genes that regulate the development of cones and rods. Our work will contribute to the understanding of human retinal development and is a framework for hypothesis generation. RPE and photoreceptor cells are promising in the treatment of retinal disease, however, several fundamental questions should be solved, such as the source of the cells, cell isolation, maturation and implanta-

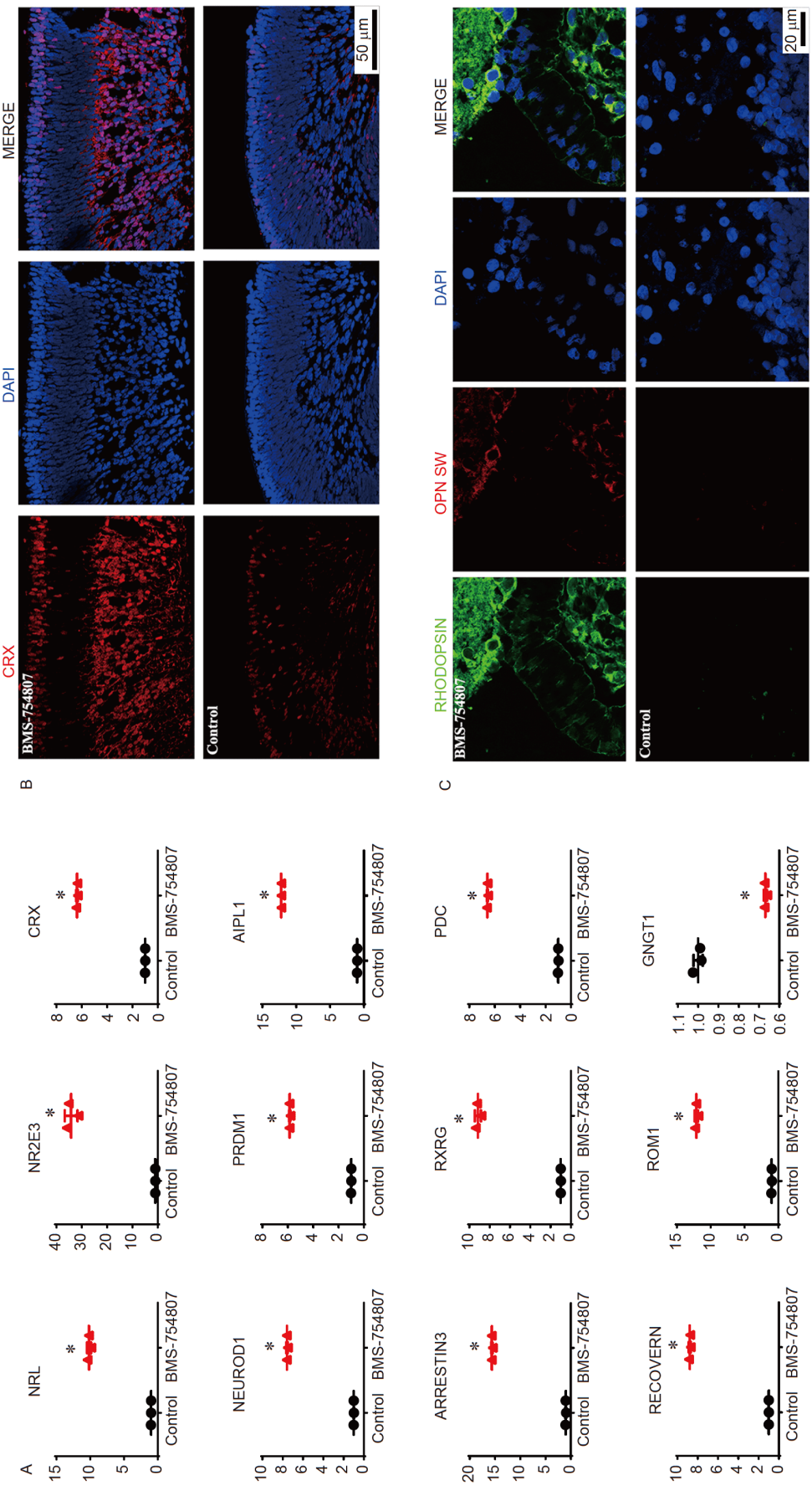

Figure 8 Blocking INSR enhances the development of photoreceptor cells in retinal organoids. A, Real-time PCR assay of NRL, NR2E3, CRX, NEUROD1, PRDM1, AIPL1, ARRESTIN3, RXRG, PDC, RECOVERIN, ROM1 and GNGT1. B, CRX (red) immunostaining of the retinal organoid in BMS-754807 treated group and control group. C, RHODOPSIN (green) and OPN SW (red) double-immunostaining of the retinal organoid in BMS-754807 treated group and control group.

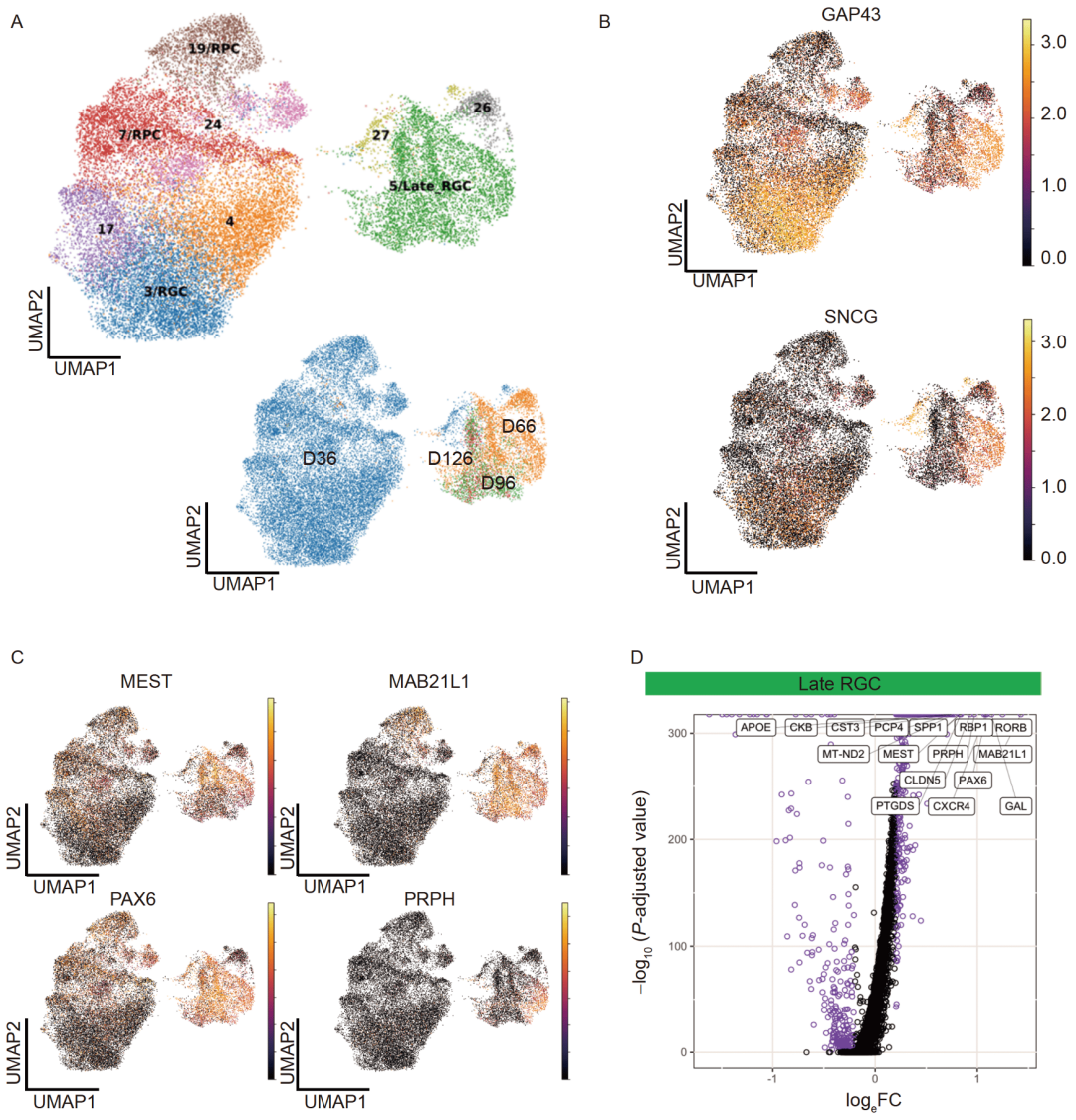

Figure 9 Subset analysis of RGCs from human retinal organoids. A, UMAP plot of the subset of RGC cluster labeled by clusters and sample timepoints. B, Feature plots showing the expression of GAP43 and SNCG, highlighting two different populations with the more mature one preferentially expressing SNCG. C, Feature plots of DE genes from DE analysis (D, volcano plot) of the Late RGC cluster versus all the other RGC clusters showing preferential expression of MEST, MAB21AL1, PAX6, and PRPH.

tion into the host (Stern et al., 2018). As the RPE cells have pigments, it is very easy to distinguish these cells from the cells in the retinal organoid, and they are widely used to treat retinal disease. However, the research on the cell signaling regulation of RPE genesis and maturation has not been fully explored. In our work, we traced the genesis and maturation of RPE cells. This information will be beneficial for choosing which stage of RPE cells as seeds.

Regarding photoreceptors, researchers have unsuccessfully tried many methods to isolate photoreceptor precursors (Carter et al., 2009; Krzyzanowski and Andrade-Navarro, 2007; Lakowski et al., 2015; Lakowski et al., 2011; Sun et al., 2009; Zhou et al., 2015). The main limitation is the lack of an appropriate model to characterize this transitioning cell type. We were able to identify immature photoreceptor populations that start to arise from D66 in the human retinal organoids. We also identified specific markers, such as CD24 and the previously predicted KCVN*2* (Kaewkhaw et al., 2015). Moreover, we identified the genes implicated in the differentiation of photoreceptor progenitors into rods and cones.

Interestingly, we identified the specific expression of INSR in this PC population. A previous study has identified the expression of INSR in the retina (Hitchcock et al., 2001; Otteson et al., 2002), and INSR is involved in the neurogenesis and neural differentiation in retinal development. After blocking the INSR with a specific antagonist, we demonstrated that INSR has robust effects on the development

of photoreceptor cells based on gene expression data. Blocking INSR from D66 could enhance the development of photoreceptor cells, this finding will be beneficial for the improvement of the PC conditional culture medium. A previous study found that the overexpression of NEUROD1 is important for retinal progenitor cells to exit cell cycle and enter the photoreceptor lineage (Ochocinska and Hitchcock, 2009). In our work, we found the upregulation of NEUROD1 after blocking INSR. However, the molecular signaling pathway requires further study.

Single-cell atlases are optimal references for engineering. scRNA-seq could unbiasedly analyzed cellular heterogeneity at different time points during differentiation. scRNAseq technologies have greatly boosted the generating of cell atlases of both mouse and human (Han et al., 2020; Rosenberg et al., 2018; Rozenblatt-Rosen et al., 2017; Sun et al., 2019). These reference maps may serve as a basis for understanding human physiology and pathology. Atlas efforts can also be applied in cell and tissue engineering. In our work, we have shown the dynamic maturation of RPE, photoreceptor, ganglion cells, and these results will help select the cell types at various time points. For instance, we may need to isolate the photoreceptor precursor cells at a day between 66 and 96 since the majority of precursors for the populations are in that specific period. Taken together, scRNA-seq will contribute to the understanding of the development of human retina.

MATERIALS AND METHODS

Maintenance of hESCs

Human embryonic stem cell line (H9) was gifted by Stem Cell Bank, Chinese Academy of Sciences (Beijing, China). The hESC line was maintained in mTeSR1 (Stem Cell Technologies, Canada) under feeder free conditions containing 5% CO_2. For passaging, hESCs colonies were washed twice with DPBS (Life Technology, USA) and treated with Versene (Life Technology) at 37°C for 5 min, then broken into smaller pieces by gentle pipetting, and resuspended with mTeSR1 culture medium and 10 mmol L^{-1} ROCK inhibitor Y27632 (R&D, USA). 24 h later, culture medium was replaced with the one without Y27632. The passages were performed at a 1:6 split ratio every 3rd day.

Retinal organoid differentiation from hESCs

The protocol we used was previously reported (Kuwahara et al., 2015) with minor modifications. From day 24, aggregates were cultured in suspension under the following 40% O_2/5% CO_2 conditions (30 aggregates/10-cm dish) the NR-differentiation medium contains DMEM/F12-Glutamax medium (Gibco, USA), 1% N2 supplement (Gibco), 10% KSR, 0.5 mmol L^{-1} retinoic acid (Sigma, USA), and 0.1 m mol L^{-1} taurine (Sigma). Retinal organoid continuously grew under these conditions for the next several weeks.

Immunofluorescence of hESCs

H9 hESCs were plated on a Germany glass cover slip, cultured for 2 days, fixed by paraformaldehyde for 30 min, and washed three times with PBS at 5 min interval. Then immunocytofluorescense was performed as described previously (Wang et al., 2014). Primary antibodies from Abcam (USA) include: Rabbit anti-OCT4, Mouse anti-Tra-1-60, Rabbit anti-SOX2, Mouse anti-SSEA4, first antibodies were all diluted at 1:250. The secondary antibodies were Alexa Fluor 488-conjugated goat anti-rabbit or mouse IgG (Molecular Probes, USA). Counter nuclear staining was performed with 4,6-diamidino-2-phenylindole (Sigma). Stained sections were analyzed with an FV3000 confocal microscope (Olympus, Japan).

Multiplex immunofluorescence of retinal organoids

The retinal organoids were fixed at day 18, 36, 66, 96 and 126 by paraformaldehyde for 30 min and embedded in paraffin, and cut for 5 μm sections. Dewaxed slices were immersed in 10 mmol L^{-1} citric acid buffer (pH 6.0, 100°C) for 25 min. Multiplex immunofluorescence with PANO 4-plex IHC kit (Panovue, Beijing, China) was performed according to the manufacture's instruction. Primary antibodies used in this study were all from Abcam: Rabbit anti-RAX, Rabbit anti-PAX6, Mouse anti-MITF, Rabbit anti-GAP43, Rabbit anti-SOX2, Rabbit anti-CRX, Rabbit anti-GFAP. Images were acquired using an FV3000 confocal microscope (Olympus).

Blocking the INSR and real time PCR

The INSR antagonist BMS-754807 (Selleck, USA) was applied at 0.1 μmol L^{-1} at D66 od retinal organoid and changed every 3 days for fresh medium with the 1 μmol L^{-1} BMS-754807. Samples were collected at D96, one part was fixed with 4% paraformaldehyde and the other part was used for mRNA extracting. cDNA reverse synthesis and Real time PCR were performed according to the manufacture's manual (Bio-Rad, USA). The primers are listed in Table S1 in Supporting Information.

Single cell cDNA library preparation and sequencing

Twenty retinal organoid at different time points (D36, D66, D96, D126, D186) post differentiation process were harvested, pooled, digested and resuspended at 1×10^6 cells per milliliter in PBS. Then the process were performed as pre-

viously reported (Qiu et al., 2017).

Quantification and statistical analysis

Single cell data preprocess

We assessed the quality of raw sequencing data by FastQC software. Trimmed fastq sequence was processed by Cell Ranger count pipeline 2.0.1 and single cell matrix was generated for each sample. All the matrixes were merged together by Seurat R package (Butler et al., 2018).

Clustering analysis

Feature selection was performed by calculating the top genes ranked by dispersion across 15 bins of gene expression distribution. These features were then adjusted for the percentage of mitochondrial genes per cell and total number of unique molecular identifier (UMI). Principal component analysis (PCA) was performed using the 2,000 most variable genes, with their scaled values. The number of principal components was determined by an Elbow plot. The gene loadings of these top principal components were analyzed, and those with genes with high variance between cells were removed. Then, a nearest neighbor network was created with the Euclidean distances between all nodes (cells) with a designated number of neighbors. Gene expression data were adjusted for total UMI counts per cell and percentage of mitochondrial genes per cell. UMAP for dimension reduction were then performed on the top principal components with default parameters to visualize cells in a two-dimensional space. Clustering analysis was then performed with Louvain algorithm incorporated into Seurat R package (Butler et al., 2018). Cell type markers were generated with Find Markers function from Seurat, and each cluster was then assessed for unique gene markers associated with known retinal cell types.

Cell subcluster analysis

To identify subpopulations within a cell type, we implemented Scanpy python package (Wolf et al., 2018). Data were subsetted for the population of interested, and cells were reclustered using the UMAP algorithm. We then performed a partitioned approximate graph abstraction (PAGA) to estimate the connectivity between the subclusters based on similarity of gene expression. Then, for graph denoising, we represented the data in a diffusion map space. After this step, embeddings were recomputed by UMAP using the PAGA-initializations.

The PAGA network was secondary analyzed with a Cytoscape Network Analyzer (Carlin et al., 2017). Through network propagation analysis, the nodes closer to the mature cell cluster of interest were selected and linked together to create groups of clusters with known differentiation lineage trajectories.

Single cell trajectory analysis

Single cell trajectory was analyzed using a subset matrix of cells and gene expressions in SCORPIUS R package (Wolf et al., 2018). Dimensionality reduction was done by using Pearson's correlation. Candidate gene markers (P value<0.05) were selected and grouped into modules based on dynamic gene expression similarity for visualization in the trajectory heatmap.

Gene enrichment analysis

Enrichments were performed by using Gene Ontology Cellular Processes and ARCHS4 Kinases databases. The online tool Enricher was used to perform these analyses (Chen et al., 2013).

Cell-cell interaction map

Ligand receptor interaction map was performed with CellphoneDB 2.0 R Package (Vento-Tormo et al., 2018), and top ligand receptor pairs were selected by P value and plotted into chord plots using the ITALK R Package (Wang et al., 2019).

Statistical analysis

All data are presented as the means±SD. Student's t-test was performed to compare the differences between groups. P<0.05 was considered statistically significant.

Compliance and ethics *The author(s) declare that they have no conflict of interest.*

Acknowledgements *This work was supported by the National Key Research and Development Program (2018YFA0107303), the National Natural Science Foundation of China (82070990), Initiation Fund of Distinguished Professor, Zhengzhou University (32310180), China Postdoctoral Research Fund (2017M613396).*

References

Berson, D. (2003). Strange vision: ganglion cells as circadian photoreceptors. Trends Neurosci 26, 314–320.

Butler, A., Hoffman, P., Smibert, P., Papalexi, E., and Satija, R. (2018). Integrating single-cell transcriptomic data across different conditions, technologies, and species. Nat Biotechnol 36, 411–420.

Butler, J.M., Sharif, U., Ali, M., McKibbin, M., Thompson, J.P., Gale, R., Yang, Y.C., Inglehearn, C., and Paraoan, L. (2015). A missense variant in *CST3* exerts a recessive effect on susceptibility to age-related macular degeneration resembling its association with Alzheimer's disease. Hum Genet 134, 705–715.

Camp, J.G., Wollny, D., and Treutlein, B. (2018). Single-cell genomics to guide human stem cell and tissue engineering. Nat Methods 15, 661–667.

Carlin, D.E., Demchak, B., Pratt, D., Sage, E., and Ideker, T. (2017). Network propagation in the cytoscape cyberinfrastructure. PLoS Comput Biol 13, e1005598.

Carter, D.A., Dick, A.D., and Mayer, E.J. (2009). $CD133^{+}$ adult human retinal cells remain undifferentiated in Leukaemia Inhibitory Factor (LIF). BMC Ophthalmol 9, 1.

Chen, E.Y., Tan, C.M., Kou, Y., Duan, Q., Wang, Z., Meirelles, G., Clark, N.R., and Ma'ayan, A. (2013). Enrichr: interactive and collaborative

HTML5 gene list enrichment analysis tool. BMC Bioinf 14, 128.
Collin, J., Queen, R., Zerti, D., Dorgau, B., Hussain, R., Coxhead, J., Cockell, S., and Lako, M. (2019). Deconstructing retinal organoids: single cell RNA-Seq reveals the cellular components of human pluripotent stem cell-derived retina. Stem Cells 37, 593–598.
da Cruz, L., Fynes, K., Georgiadis, O., Kerby, J., Luo, Y.H., Ahmado, A., Vernon, A., Daniels, J.T., Nommiste, B., Hasan, S.M., et al. (2018). Phase 1 clinical study of an embryonic stem cell-derived retinal pigment epithelium patch in age-related macular degeneration. Nat Biotechnol 36, 328–337.
De Cat, B., Muyldermans, S.Y., Coomans, C., Degeest, G., Vanderschueren, B., Creemers, J., Biemar, F., Peers, B., and David, G. (2003). Processing by proprotein convertases is required for glypican-3 modulation of cell survival, Wnt signaling, and gastrulation movements. J Cell Biol 163, 625–635.
Dulken, B.W., Leeman, D.S., Boutet, S.C., Hebestreit, K., and Brunet, A. (2017). Single-cell transcriptomic analysis defines heterogeneity and transcriptional dynamics in the adult neural stem cell lineage. Cell Rep 18, 777–790.
Farrell, J.A., Wang, Y., Riesenfeld, S.J., Shekhar, K., Regev, A., and Schier, A.F. (2018). Single-cell reconstruction of developmental trajectories during zebrafish embryogenesis. Science 360, eaar3131.
Gonzalez-Cordero, A., Kruczek, K., Naeem, A., Fernando, M., Kloc, M., Ribeiro, J., Goh, D., Duran, Y., Blackford, S.J.I., Abelleira-Hervas, L., et al. (2017). Recapitulation of human retinal development from human pluripotent stem cells generates transplantable populations of cone photoreceptors. Stem Cell Rep 9, 820–837.
Han, X., Wang, R., Zhou, Y., Fei, L., Sun, H., Lai, S., Saadatpour, A., Zhou, Z., Chen, H., Ye, F., et al. (2018). Mapping the mouse cell atlas by microwell-seq. Cell 172, 1091–1107.e17.
Han, X., Zhou, Z., Fei, L., Sun, H., Wang, R., Chen, Y., Chen, H., Wang, J., Tang, H., Ge, W., et al. (2020). Construction of a human cell landscape at single-cell level. Nature 581, 303–309.
Hitchcock, P.F., Otteson, D.C., and Cirenza, P.F. (2001). Expression of the insulin receptor in the retina of the goldfish. Invest Ophthalmol Vis Sci 42, 2125–2129.
Hu, Y., Wang, X., Hu, B., Mao, Y., Chen, Y., Yan, L., Yong, J., Dong, J., Wei, Y., Wang, W., et al. (2019). Dissecting the transcriptome landscape of the human fetal neural retina and retinal pigment epithelium by single-cell RNA-seq analysis. PLoS Biol 17, e3000365.
Kaewkhaw, R., Kaya, K.D., Brooks, M., Homma, K., Zou, J., Chaitankar, V., Rao, M., and Swaroop, A. (2015). Transcriptome dynamics of developing photoreceptors in three-dimensional retina cultures recapitulates temporal sequence of human cone and rod differentiation revealing cell surface markers and gene networks. Stem Cells 33, 3504–3518.
Kim, S., Lowe, A., Dharmat, R., Lee, S., Owen, L.A., Wang, J., Shakoor, A., Li, Y., Morgan, D.J., Hejazi, A.A., et al. (2019). Generation, transcriptome profiling, and functional validation of cone-rich human retinal organoids. Proc Natl Acad Sci USA 116, 10824–10833.
Klein, A.M., Mazutis, L., Akartuna, I., Tallapragada, N., Veres, A., Li, V., Peshkin, L., Weitz, D.A., and Kirschner, M.W. (2015). Droplet barcoding for single-cell transcriptomics applied to embryonic stem cells. Cell 161, 1187–1201.
Krzyzanowski, P.M., and Andrade-Navarro, M.A. (2007). Identification of novel stem cell markers using gap analysis of gene expression data. Genome Biol 8, R193.
Kuwahara, A., Ozone, C., Nakano, T., Saito, K., Eiraku, M., and Sasai, Y. (2015). Generation of a ciliary margin-like stem cell niche from self-organizing human retinal tissue. Nat Commun 6, 6286.
La Manno, G., Gyllborg, D., Codeluppi, S., Nishimura, K., Salto, C., Zeisel, A., Borm, L.E., Stott, S.R.W., Toledo, E.M., Villaescusa, J.C., et al. (2016). Molecular diversity of midbrain development in mouse, human, and stem cells. Cell 167, 566–580.e19.
Laboissonniere, L.A., Goetz, J.J., Martin, G.M., Bi, R., Lund, T.J.S., Ellson, L., Lynch, M.R., Mooney, B., Wickham, H., Liu, P., et al. (2019). Molecular signatures of retinal ganglion cells revealed through single cell profiling. Sci Rep 9, 15778.
Lakowski, J., Han, Y.T., Pearson, R.A., Gonzalez-Cordero, A., West, E.L., Gualdoni, S., Barber, A.C., Hubank, M., Ali, R.R., and Sowden, J.C. (2011). Effective transplantation of photoreceptor precursor cells selected via cell surface antigen expression. Stem Cells 29, 1391–1404.
Lakowski, J., Gonzalez-Cordero, A., West, E.L., Han, Y.T., Welby, E., Naeem, A., Blackford, S.J.I., Bainbridge, J.W.B., Pearson, R.A., Ali, R. R., et al. (2015). Transplantation of photoreceptor precursors isolated via a cell surface biomarker panel from embryonic stem cell-derived self-forming retina. Stem Cells 33, 2469–2482.
Liu, Y., Fan, X., Wang, R., Lu, X., Dang, Y.L., Wang, H., Lin, H.Y., Zhu, C., Ge, H., Cross, J.C., et al. (2018). Single-cell RNA-seq reveals the diversity of trophoblast subtypes and patterns of differentiation in the human placenta. Cell Res 28, 819–832.
Macosko, E.Z., Basu, A., Satija, R., Nemesh, J., Shekhar, K., Goldman, M., Tirosh, I., Bialas, A.R., Kamitaki, N., Martersteck, E.M., et al. (2015). Highly parallel genome-wide expression profiling of individual cells using nanoliter droplets. Cell 161, 1202–1214.
Mao, X., An, Q., Xi, H., Yang, X.J., Zhang, X., Yuan, S., Wang, J., Hu, Y., Liu, Q., and Fan, G. (2019). Single-cell RNA sequencing of hESC-derived 3D retinal organoids reveals novel genes regulating RPC commitment in early human retinogenesis. Stem Cell Rep 13, 747–760.
Nakano, T., Ando, S., Takata, N., Kawada, M., Muguruma, K., Sekiguchi, K., Saito, K., Yonemura, S., Eiraku, M., and Sasai, Y. (2012). Self-formation of optic cups and storable stratified neural retina from human ESCs. Cell Stem Cell 10, 771–785.
Ochocinska, M.J., and Hitchcock, P.F. (2009). NeuroD regulates proliferation of photoreceptor progenitors in the retina of the zebrafish. Mech Dev 126, 128–141.
Otteson, D.C., Cirenza, P.F., and Hitchcock, P.F. (2002). Persistent neurogenesis in the teleost retina: evidence for regulation by the growth-hormone/insulin-like growth factor-I axis. Mech Dev 117, 137–149.
Paul, F., Arkin, Y., Giladi, A., Jaitin, D.A., Kenigsberg, E., Keren-Shaul, H., Winter, D., Lara-Astiaso, D., Gury, M., Weiner, A., et al. (2015). Transcriptional heterogeneity and lineage commitment in myeloid progenitors. Cell 163, 1663–1677.
Peng, Y.R., Shekhar, K., Yan, W., Herrmann, D., Sappington, A., Bryman, G.S., van Zyl, T., Do, M.T.H., Regev, A., and Sanes, J.R. (2019). Molecular classification and comparative taxonomics of foveal and peripheral cells in primate retina. Cell 176, 1222–1237.e22.
Phillips, M.J., Jiang, P., Howden, S., Barney, P., Min, J., York, N.W., Chu, L.F., Capowski, E.E., Cash, A., Jain, S., et al. (2018). A novel approach to single cell RNA-sequence analysis facilitates *in silico* gene reporting of human pluripotent stem cell-derived retinal cell types. Stem Cells 36, 313–324.
Qiu, X., Hill, A., Packer, J., Lin, D., Ma, Y.A., and Trapnell, C. (2017). Single-cell mRNA quantification and differential analysis with Census. Nat Methods 14, 309–315.
Rosenberg, A.B., Roco, C.M., Muscat, R.A., Kuchina, A., Sample, P., Yao, Z., Graybuck, L.T., Peeler, D.J., Mukherjee, S., Chen, W., et al. (2018). Single-cell profiling of the developing mouse brain and spinal cord with split-pool barcoding. Science 360, 176–182.
Rozenblatt-Rosen, O., Stubbington, M.J.T., Regev, A., and Teichmann, S. A. (2017). The Human Cell Atlas: from vision to reality. Nature 550, 451–453.
Schwartz, S.D., Regillo, C.D., Lam, B.L., Eliott, D., Rosenfeld, P.J., Gregori, N.Z., Hubschman, J.P., Davis, J.L., Heilwell, G., Spirn, M., et al. (2015). Human embryonic stem cell-derived retinal pigment epithelium in patients with age-related macular degeneration and Stargardt's macular dystrophy: follow-up of two open-label phase 1/2 studies. Lancet 385, 509–516.
Shekhar, K., Lapan, S.W., Whitney, I.E., Tran, N.M., Macosko, E.Z., Kowalczyk, M., Adiconis, X., Levin, J.Z., Nemesh, J., Goldman, M., et al. (2016). Comprehensive classification of retinal bipolar neurons by single-cell transcriptomics. Cell 166, 1308–1323.e30.

Shen, Y., Shen, H., Guo, D., Sun, X., Sun, Y., Hong, N., Wang, X., Xie, C., Zhao, Y., He, Q., et al. (2020). Recent developments in regenerative ophthalmology. Sci China Life Sci 63, 1450–1490.
Stern, J.H., Tian, Y., Funderburgh, J., Pellegrini, G., Zhang, K., Goldberg, J.L., Ali, R.R., Young, M., Xie, Y., and Temple, S. (2018). Regenerating eye tissues to preserve and restore vision. Cell Stem Cell 23, 453.
Sun, H., Zhou, Y., Fei, L., Chen, H., and Guo, G. (2019). scMCA: A tool to define mouse cell types based on single-cell digital expression. In: In: Yuan, G.C., ed. Computational Methods for Single-Cell Data Analysis. Methods in Molecular Biology. New York: Humana Press, 91–96.
Sun, Y., Kong, W., Falk, A., Hu, J., Zhou, L., Pollard, S., and Smith, A. (2009). CD133 (Prominin) negative human neural stem cells are clonogenic and tripotent. PLoS ONE 4, e5498.
Tasic, B., Menon, V., Nguyen, T.N., Kim, T.K., Jarsky, T., Yao, Z., Levi, B., Gray, L.T., Sorensen, S.A., Dolbeare, T., et al. (2016). Adult mouse cortical cell taxonomy revealed by single cell transcriptomics. Nat Neurosci 19, 335–346.
Treutlein, B., Brownfield, D.G., Wu, A.R., Neff, N.F., Mantalas, G.L., Espinoza, F.H., Desai, T.J., Krasnow, M.A., and Quake, S.R. (2014). Reconstructing lineage hierarchies of the distal lung epithelium using single-cell RNA-seq. Nature 509, 371–375.
Vento-Tormo, R., Efremova, M., Botting, R.A., Turco, M.Y., Vento-Tormo, M., Meyer, K.B., Park, J.E., Stephenson, E., Polański, K., Goncalves, A., et al. (2018). Single-cell reconstruction of the early maternal-fetal interface in humans. Nature 563, 347–353.
Völkner, M., Zschätzsch, M., Rostovskaya, M., Overall, R.W., Busskamp, V., Anastassiadis, K., and Karl, M.O. (2016). Retinal organoids from pluripotent stem cells efficiently recapitulate retinogenesis. Stem Cell Rep 6, 525–538.
Wagner, D.E., Weinreb, C., Collins, Z.M., Briggs, J.A., Megason, S.G., and Klein, A.M. (2018). Single-cell mapping of gene expression landscapes and lineage in the zebrafish embryo. Science 360, 981–987.
Wang, S.J., Weng, C.H., Xu, H.W., Zhao, C.J., and Yin, Z.Q. (2014). Effect of optogenetic stimulus on the proliferation and cell cycle progression of neural stem cells. J Membr Biol 247, 493–500.
Wang, Y., Wang, R., Zhang, S., Song, S., Jiang, C., Han, G., Wang, M., Ajani, J., Futreal, A., and Wang, L. (2019). iTALK: an R package to characterize and illustrate intercellular communication. bioRxiv, 507871.
Wolf, F.A., Angerer, P., and Theis, F.J. (2018). SCANPY: large-scale single-cell gene expression data analysis. Genome Biol 19, 15.
Wu, B., An, C., Li, Y., Yin, Z., Gong, L., Li, Z., Liu, Y., Heng, B.C., Zhang, D., Ouyang, H., et al. (2017). Reconstructing lineage hierarchies of mouse uterus epithelial development using single-cell analysis. Stem Cell Rep 9, 381–396.
Yao, Z., Mich, J.K., Ku, S., Menon, V., Krostag, A.R., Martinez, R.A., Furchtgott, L., Mulholland, H., Bort, S., Fuqua, M.A., et al. (2017). A single-cell roadmap of lineage bifurcation in human ESC models of embryonic brain development. Cell Stem Cell 20, 120–134.
Zeisel, A., Munoz-Manchado, A.B., Codeluppi, S., Lonnerberg, P., La Manno, G., Jureus, A., Marques, S., Munguba, H., He, L., Betsholtz, C., et al. (2015). Cell types in the mouse cortex and hippocampus revealed by single-cell RNA-seq. Science 347, 1138–1142.
Zeisel, A., Hochgerner, H., Lönnerberg, P., Johnsson, A., Memic, F., van der Zwan, J., Häring, M., Braun, E., Borm, L.E., La Manno, G., et al. (2018). Molecular architecture of the mouse nervous system. Cell 174, 999–1014.e22.
Zhong, S., Zhang, S., Fan, X., Wu, Q., Yan, L., Dong, J., Zhang, H., Li, L., Sun, L., Pan, N., et al. (2018). A single-cell RNA-seq survey of the developmental landscape of the human prefrontal cortex. Nature 555, 524–528.
Zhou, F., Li, X., Wang, W., Zhu, P., Zhou, J., He, W., Ding, M., Xiong, F., Zheng, X., Li, Z., et al. (2016). Tracing haematopoietic stem cell formation at single-cell resolution. Nature 533, 487–492.
Zhou, P.Y., Peng, G.H., Xu, H., and Yin, Z.Q. (2015). c-Kit$^+$ cells isolated from human fetal retinas represent a new population of retinal progenitor cells. J Cell Sci 128, 2169–2178.
Zhu, J., Reynolds, J., Garcia, T., Cifuentes, H., Chew, S., Zeng, X., and Lamba, D.A. (2018). Generation of transplantable retinal photoreceptors from a current good manufacturing practice-manufactured human induced pluripotent stem cell Line. Stem Cells Transl Med 7, 210–219.
Zurdel, J., Finckh, U., Menzer, G., Nitsch, R.M., and Richard, G. (2002). *CST3* genotype associated with exudative age related macular degeneration. British J Ophthalmol 86, 214–219.

SUPPORTING INFORMATION

The supporting information is available online at https://doi.org/10.1007/s11427-020-1836-7. The supporting materials are published as submitted, without typesetting or editing. The responsibility for scientific accuracy and content remains entirely with the authors.